Closed Loop Control of a Wing's Lift for 'Gust' Suppression

Wesley Kerstens[1] and David Williams[2]
Illinois Institute of Technology, Chicago, IL, 60616

Jens Pfeiffer[3] and Rudibert King[4]
Technische Universität Berlin, Berlin, Germany

and

Tim Colonius[5]
California Institute of Technology, Pasadena, CA, 91125

The ability to maintain a constant lift force on a low aspect ratio semi circular wing using pulsed blowing active flow control is experimentally investigated. Dynamic models of the wing's response to pressure (pulsed blowing) actuation and the response to longitudinal gusting are obtained through black-box system identification methods. Robust closed loop controllers are synthesized using a mixed sensitivity loop shaping approach. An additional feedforward disturbance compensation is designed based on a model of the unsteady aerodynamics. The controllers show good suppression of lift fluctuations at low frequencies, but as frequencies increase the control performance degrades due to fundamental physical limitations. The limitations are related to the leading edge vortex formation time.

Nomenclature

L	=	lift force [N], perpendicular to flow direction
D	=	drag force [N], aligned with flow direction
U	=	flow speed [m/s]
c	=	chord length [m]
t^+	=	dimensionless time = tU/c
α	=	wing angle of attack
f	=	frequency [Hz]
St	=	Strouhal number = fc/U
k	=	reduced frequency = $\pi fc/U$

I. Introduction

Active flow control has the ability to delay separation or force reattachment of a separated flow over a surface. For example, Darbi and Wygnanski[1] showed substantial increases in the normal force coefficient on a flap by periodic excitation of the flow at the flap shoulder with a voice coil driven actuator. Glezer[2] showed increases in the circulation using pulsed-combustion actuators located on the suction side of an airfoil. Williams et. al.[3] showed increases in the lift coefficient of a three-dimensional wing used pulsed-blowing jets located along the leading edge. Regardless of the geometry, actuator type or actuator location (all actuation is applied near the separation point), all show a similar step or impulse response to actuation. After the onset of actuation an initial decrease in the lift

[1] Graduate Research Assistant, Mechanical and Aerospace Engineering Department, AIAA Student Member.
[2] Professor, Mechanical and Aerospace Engineering Department, AIAA Associate Fellow.
[3] Graduate Research Assistant, Measurement and Control Group, AIAA Student Member.
[4] Professor, Measurement and Control Group, AIAA Member.
[5] Professor, Mechanical Engineering Department, AIAA Associate Fellow.

(minimum observed at $t^+ \approx 1$-2) is observed followed by an increase to a maximum value and in Ref. 2-3 a slow relaxation back to the steady state value. The mechanism of reattachment is described well in Ref. 1.

Most active flow control work has considered only the steady state response to actuation. For practical implementation of AFC in uses for gust suppression or replacement of conventional control surfaces, an understanding of the dynamics associated with actuation is necessary. A mathematical model describing the time varying response to actuation is necessary for basic closed loop control development. The complex interaction between the actuators and flow field is not easily modeled and requires simplified models to describe the dynamics for applications in real-time control applications.

In addition to understanding the dynamics associated with AFC an understanding of the response of a flight vehicle to a time varying external flow field is necessary for practical implementation of AFC in flight vehicles. The response to longitudinal gusting was studied by Greenberg[4], which was a slight extension to Theodorsen's[5] theory. The theories are limited by their assumptions of two-dimensional attached flow and the assumption of a thin, planar wake. Both of these assumptions are clearly violated when dealing with low aspect ratio wings and separated flow. Greenberg's theory predicts that the lift leads the velocity at low frequencies (k<0.3) and as the frequency increases the added mass term dominates and the phase between the lift and velocity asymptotically approaches a lag of 90 degrees. Measurements of the phase between the velocity and lift on a low aspect ratio wing[6] show similar trends at low frequencies but a much larger phase lead than predicted by Greenberg. The amplitude of lift fluctuations, predicted by Greenberg, decreases as the frequency increases. Measurements of the amplitude with attached flow agree with the theory, but with separated flow the amplitude of lift fluctuations increases as the frequency increases. The increasing lift amplitude is related to dynamic stall vortices formed during the acceleration and deceleration of the flow. Leishman[7] and van der Wall[8] offer good descriptions of the limitations and values of the various unsteady aerodynamic theories.

An early attempt at controlling lift oscillations was investigated by Williams et. al.[6]. The experimentally determined phase between the velocity fluctuations and the lift and the resulting amplitudes were used to develop a point frequency suppression controller, which delays the measured velocity signal by the measured time delay, this showed substantial suppression of a sinusoidally oscillating freestream at 1Hz. Although effective at suppressing oscillations at a single frequency, this type of feedforward controller is unable to respond to arbitrary velocity variations, i.e., real gusting conditions.

In Ref. 9 using the lift coefficient and the square root of the jet pressure to model the plant dynamics a robust closed-loop controller was designed which is able to compensate for arbitrary disturbances within a certain bandwidth. This controller required the computation of a reference lift coefficient as the set point, which varied as the freestream velocity varied. The lift coefficient was obtained by dividing a desired lift by the instantaneous square of the velocity. The input and output variables, C_L and $C_{pj}^{1/2}$, were chosen because it collapses the data across varying freestream speeds to a single "linear" curve, allowing for less complex closed loop controller synthesis techniques to be employed. The frequency range in which this controller is efficient is limited to quasi-steady conditions, i.e. low frequency velocity fluctuations, due to un-modeled unsteady aerodynamics. In the higher frequency range the lift force fluctuations lead the velocity fluctuations. In addition, the ratio of lift amplitude to velocity amplitude is a function of frequency. The dynamics associated with the time varying velocity cause incorrect computations of the reference lift coefficient so although the closed loop system showed good tracking response of the lift coefficient, when converted to lift force the closed loop system showed good performance at low frequencies (k<0.05) but limited control at higher frequencies.

The current work concentrates on using AFC to suppress lift fluctuations about a mean flow speed, treated as a "cruise" flight condition using the lift force as the output/feedback variable. The incorporation of an unsteady aerodynamic model and feedforward disturbance compensation based on this unsteady aerodynamic model are used to speed up the response of the suppression of lift fluctuations. The experimental setup is described in section II. The modeling of the dynamic response to actuation and unsteady aerodynamics are described in section III along with the controller synthesis methods and the results of the closed loop control experiments. Section IV discusses the results and the limitations imposed by the dynamic response.

II. Experimental Setup

The experiments were conducted in the Andrew Fejer Unsteady Flow Wind Tunnel at Illinois Institute of Technology. The wind tunnel is a closed-return type powered by a 40 HP motor with a vector drive controller. Figure 1 shows a schematic of the wind tunnel test section with the model mounted on its sting. The test section dimensions are 0.61m by 0.61m with a length of 3.1m. Flow speeds used during the experiments ranged from 4m/s to 9m/s. The highest level of freestream turbulence level was measured to be 0.6 percent at an average speed of 3

m/s and over a bandwidth from 0.1 Hz to 30 Hz. A computer-controlled cascade of shutters located at the downstream end of the test section is used to control the freestream speed oscillations. Oscillation amplitudes up to 10 percent of the mean speed and frequencies up to 3 Hz are achievable. Mean flow velocities are measured with a pitot-static tube and dynamic velocities are measured with a hotwire anemometer, both located approximately 1m upstream of the wing. The forces and moments acting on the wing are recorded with a 6-component balance (ATI - Nano 17). The uncertainty in the force measurement is based on the repeatability of calibration data and is estimated to be less than 0.01 N.

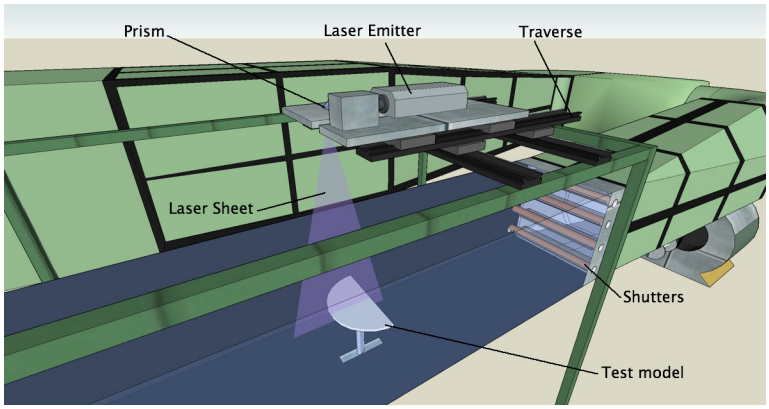

Figure 1. Schematic of Andrew Fejer Unsteady Wind Tunnel

The wing has a semicircular planform area with a centerline chord of 0.203m. The wing was constructed from Duraform® using a 3D Systems selective laser sintering, rapid prototyping machine. It is fixed at an angle of attack α=20° for all of the measurements in this study, which corresponds to a fully separated state. The flow separates at the leading edge and the separation bubble closes downstream of the trailing edge. The flow control actuator is a pulsed-blowing type. Sixteen Lee micro-valves, designed to fit into the leading edge of the wing, are positioned radially along the leading edge within the wing. A Fairchild pressure regulator (model TA-6000-004U) regulates the pressure supply to the plenum within the wing. The pressure at the regulator output is measured with an Omega Engineering® (model px139) pressure transducer. The micro-valves are operated at 29Hz (St=0.84 at 7m/s) and the pressure within the plenum is varied to change the actuation amplitude. At the maximum pressure allowed by the wing, the mass flow rate is measured to be 9.26×10^{-4} kg/s at 34.5kPa. The leading edge is tapered with a 5:1 elliptic shape, and the thickness to chord ratio is 0.069. The centerline chord-based Reynolds numbers ranged from Re_c = 62,000 to 140,000. The micro-valves, pressure regulator, shutters and data acquisition are controlled with Simulink® models, dSPACE® software and a ds1104 ADC/DAC interface running at a sample rate of 10 kHz. Force balance, velocity information and pressure data are acquired at a sampling rate of 1 kHz.

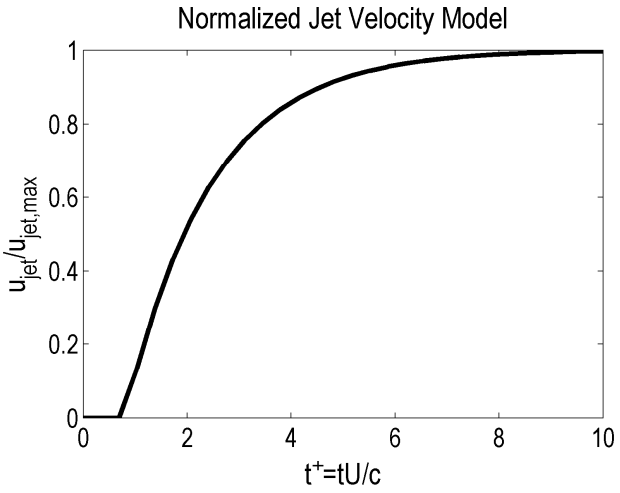

Figure 2. Normalized jet velocity response to a step increase in pressure plotted versus convective time at 7m/s. Nominal model shows time delay of 0.023 seconds (t^+=0.8)

The time response of the pulsed-blowing wing's jet velocity is limited by the pressure regulator's bandwidth, the volume of the plenum and associated plumbing. Jet velocities, measured with a hotwire anemometer located in the center of a jet located just off the centerline of the wing, exhibit a first order dynamic response with time delay. Time delays between the desired pressure input signal and the jet exit velocity, due to the time required to pressurize the plenum volume within the wing, range from 0.015sec (t^+=0.5) to 0.030sec (t^+=1). A nominal model from desired pressure to jet velocity has a time delay of 0.023sec (t^+=0.8). The model of the jet velocity is shown in figure 2, plotted as the jet velocity normalized by the maximum jet velocity against the convective time at 7m/s.

III. Results

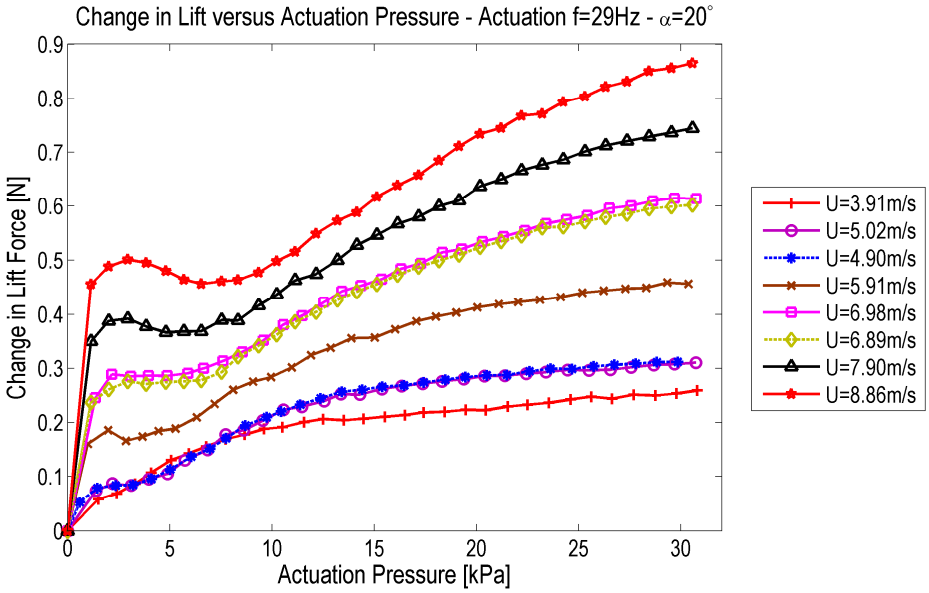

Figure 3. Pulsed blowing wing's static map of lift response to pressure actuation

A. Plant Model identification

The range of possible control is first determined by creating a static map, which is the steady state lift response to pressure actuation. The angle of attack is fixed at 20°, the micro-valves are pulsed continuously at 29Hz, and the plenum pressure is varied in 1kPa increments. Data is acquired for 60 seconds at each pressure magnitude and the mean value of the lift is found. The process is repeated for varying flow speeds. Figure 3 shows the mean lift response at flow speeds 4m/s through 9m/s with the measurements at 5m/s and 7m/s repeated as a repeatability test. The data collapses to a single "linear" curve when plotted as the change in lift coefficient versus the square root of the jet pressure coefficient, see Ref. 9.

To identify dynamic models of the wing's response to actuation, black-box system identification methods are employed. Black-box modeling requires measuring the system response to pseudo-random binary signal (PRBS) step inputs in plenum pressure. The input signal is the recorded 'desired pressure' and the output signal is the change in lift signal measured by the force balance. Herein the change in lift is defined as the deviation from the steady-state lift that corresponds to actuation at the lower pressure level. One example of the input and output measurements is shown in figure 4.

The experiments are repeated at varying magnitudes of input pressures and pressures for two flow speeds of approximately 5 m/s and 7 m/s. A family of 21 linear black-box dynamic models was identified using the

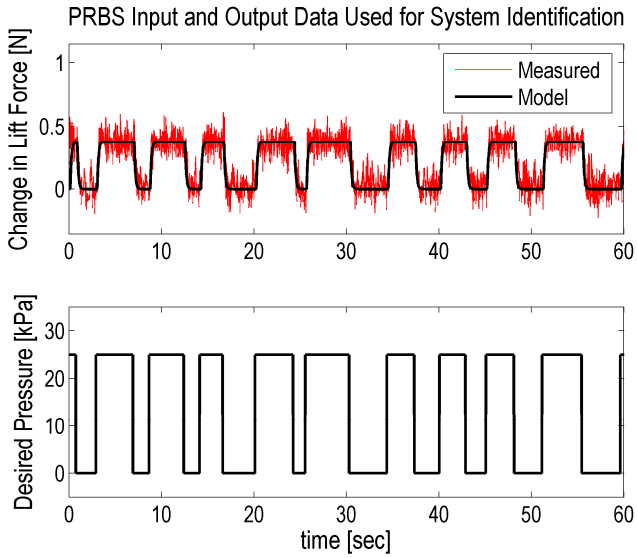

Figure 4. Example of input-output data used to obtain black-box dynamic models of response to pressure actuation. Dark line shows one of the identified models.

Prediction-Error-Method. First order models with a time delay of the form,

$$G_P(s) = \frac{k}{Ts+1} e^{-\theta s} \qquad (1)$$

fit the data well, as can be seen in figure 4 from the comparison of the measured and simulated response for one of the identified models. The consideration of the time delay results in a significantly better fit of the experimental data when compared to models identified in earlier investigations[9].

The frequency response of all identified models is shown in figure 5. Each model family identified for a fixed flow speed is characterized by a variation of parameters corresponding to the actual nonlinear response of the flow to the actuation. This relates also to the nonlinearity seen in the static maps for the different flow speeds shown in figure 3.

Furthermore the majority of the models identified at the lower flow speed of $U = 5$ m/s show a smaller gain than the ones identified at $U = 7$ m/s, which is mostly due to the fact that the plant models are defined within the scope of this paper with respect to dimensional variables. This in turn allows for an easier controller design and implementation, since the control objective is mainly to reject disturbances while maintaining a constant lift force.

The control design presented in this paper focuses on achieving good disturbance suppression at a nominal flow speed of 7 m/s. Therefore, a nominal model was found by taking the mean of only the transfer functions identified at this flow speed. In order to obtain a rational transfer function, the dead-time element corresponding to the mean time delay of $\theta = 0.157$ s is approximated by a third order all-pass transfer function. Its coefficients are determined based on a least squares method proposed by Frank[10], which minimizes the difference between the step responses of the original and the approximated transfer function. However, the approximation leads to a deviation of the phase for frequencies larger than about 6 Hz as can be seen from figure 5. This is acceptable because it lies far enough above the frequency range of interest for the controlled plant.

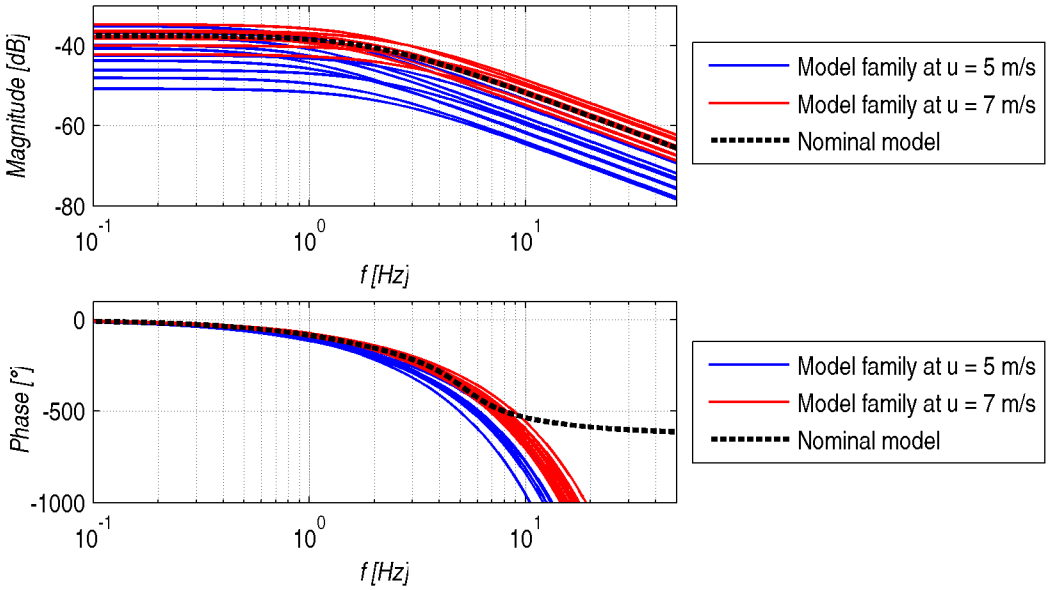

Figure 5. Frequency response diagram of identified models at flow speeds 5 m/s and 7 m/s. The dashed line is the nominal model found from the mean of the family model parameters for 7 m/s. To obtain a rational transfer function the time delay of the nominal model is approximated by an all-pass transfer function.

B. Unsteady Aerodynamic Model Identification

The wing's response to a time varying longitudinal "gusting" velocity is itself dynamic. The separated flow and the low aspect ratio of the wing do not lend themselves to any available theory so a separate black-box model is identified from experimental data. The lift response of the wing to sinusoidal velocity inputs at several frequencies is measured. The amplitude ratio of the lift force to the velocity amplitude is determined from the energy at the

fundamental frequency in the power spectrum. The phase between the resulting lift force and the velocity, from hotwire measurements, is determined from the cross power spectrum. Figure 6 shows the ratio of the lift force amplitude to the velocity amplitude, and the phase between these signals, plotted against the frequency of velocity fluctuations. The frequency response of the wing to gusting conditions is then used to identify a black-box dynamic model. The resulting model becomes the disturbance model in the control architecture; see below for a description of the control architecture. The final form of the disturbance model is also shown in figure 6.

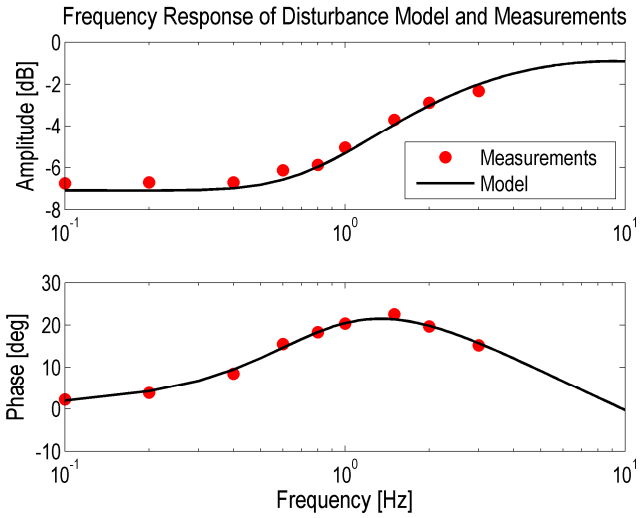

Figure 6. Unsteady aerodynamic model: frequency response of lift force to longitudinal gusting flow with a mean flow speed of 7m/s. Individual points represent measurements from sinusoidal velocity forcing and the solid line is the model generated from the frequency response measurements.

C. Controller Architecture

The main control objective is to maintain a constant lift by suppressing disturbances caused by sudden flow speed variations. This is achieved by employing a two degrees-of-freedom controller shown in figure 7. The output y_P of the plant model G_P is perturbed by a disturbance y_d. Therefore, the actual lift force y is measured and compared against the reference value r. A robust feedback controller $K(s)$ regulates the lift force by adjusting the actuation pressure p_j. The closed-loop part of the control architecture provides set-point tracking at zero steady-state error, which accounts for model uncertainties and compensates the disturbances acting on the plant at low frequencies. The synthesis of the controller is discussed in detail in section D.

The output disturbance y_d corresponding to a deviation of the lift force is caused by fluctuations in the flow speed $d = U'$. This represents the unsteady aerodynamics of the wing and can be modeled by the black-box disturbance model G_d. As the flow speed is measured online, the input d to the disturbance model is known. This information can be exploited by using a feedforward controller $K_D(s)$, which acts on the plant input u to enhance the disturbance compensation.

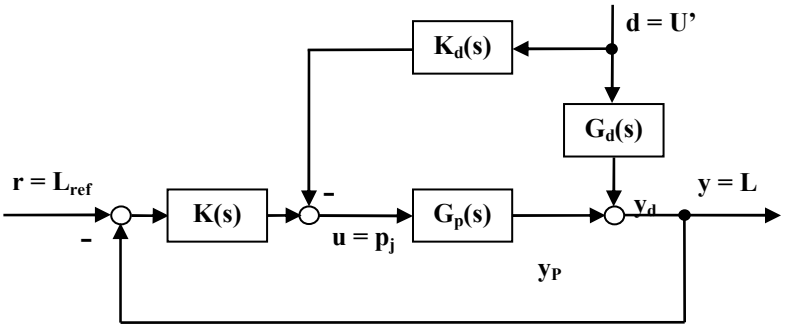

Figure 7. Controller architecture used for closed loop experiments.

To account for actuator saturation due to the limited actuation pressure the control loop is augmented with a dynamic anti-windup compensator based on a method suggested by Park[11]. It is not shown in Figure 7 for the sake of conciseness.

D. Controller Synthesis

A robust H_∞ feedback controller $K(s)$ is synthesized using the mixed-sensitivity loop-shaping approach[12]. This closed-loop control strategy has been successfully applied in several active flow-control experiments[9, 13-14] and is augmented here by a feedforward controller $K_D(s)$ for improved disturbance rejection. By choosing appropriate the

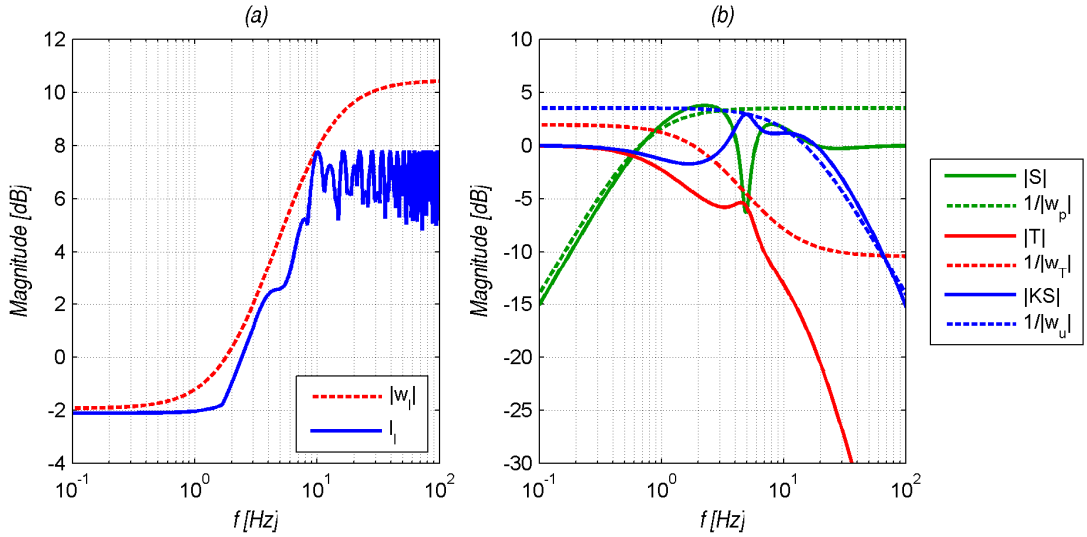

Figure 8. Multiplicative uncertainty for the identified model family (a) and loop-shaping weights with corresponding transfer functions for the synthesized H_∞-controller (b)

loop-shaping weights, the mixed-sensitivity control synthesis guarantees robust stability and performance of the closed loop for a given model family. To do so, the maximum deviation of all models $G_p(s)$ within the model family Π_I from the nominal model $G_n(s)$ is described by a multiplicative uncertainty

$$l_I(\omega) = \max_{G_P \in \Pi_I} \left| \frac{G_p(j\omega) - G(j\omega)}{G(j\omega)} \right| \qquad (2)$$

Hence, the model family can be described by

$$\Pi_I : \; G_p(s) = G_n(s)\left(1 + w_I(s)\Delta_I(s)\right), \quad \left|\Delta_I(j\omega)\right| \le 1, \quad \forall \omega \,, \qquad (3)$$

wherein $\Delta_I(s)$ denotes a normalized uncertainty with a frequency dependent weight $w_I(s)$ comprising all identified transfer functions. Figure 8 a) shows the multiplicative uncertainty $l_I(\omega)$ and the magnitude of the corresponding weight $|w_I(s)|$ for the family of models identified for the wing. The uncertainty could be reduced by inverting the static map shown in Figure 3 for one fixed flow speed and using it as a pre-compensator to account for the steady-state part of the nonlinearities. This was examined in earlier experiments by the authors[9] but turned out not to be necessary in the current control design, since the closed-loop performance is limited by the time delay of the plant transfer function. This limitation will be discussed further towards the end of this section.

To tune the controller $K(s)$ one considers the closed-loop response of the nominal plant, which is given by

$$y = \underbrace{\frac{G_n K}{1 + G_n K}}_{T} r + \underbrace{\frac{1}{1 + G_N K}}_{S} \underbrace{\left(1 - G_n K_d G_d^{-1}\right)}_{S_d} G_d d \,, \qquad (4)$$

wherein T represents the complementary sensitivity function relating to tracking performance and measurement noise. S denotes the sensitivity function relating to suppression of disturbances acting on the output of the closed loop. Finally, S_d can be interpreted as a feedforward sensitivity function[12]. The sensitivity function S and the complementary sensitivity function T are shaped by the weights $w_P(s)$ and $w_T(s)$, respectively. A third weight $w_U(s)$ is used to put a bound on the control effort KS. In order to obtain the controller a cost functional

$$\min_K \left\| N(K(s)) \right\|_\infty, \text{ with } N = \left[w_P S \quad w_T T \quad w_u K S \right]^T, \qquad (5)$$

has to be minimized, wherein $K(s)$ denotes the optimal controller[12]. The frequency response of the closed-loop transfer functions with the corresponding loop-shaping weights is shown in figure 8 b). Note that plant model was scaled to an input and output variable range during the loop-shaping process to allow for easier choice of weights. Adjusting the weight $w_T(s)$ such that

$$|T(j\omega)| < 1/|w_1(j\omega)|, \ \forall\omega, \qquad (6)$$

ensures robust stability of the closed-loop for all models identified for the flow speeds 5 m/s and 7 m/s. Note that the magnitude of the uncertainty $|w_I(s)|$ exceeds unity for frequencies larger than approximately 2 Hz. This puts an upper limit on the achievable bandwidth ω_{BT} with respect to the set-point tracking performance. However, figure 8 b) reveals that the magnitude of the complementary sensitivity T is still well below this limit. Other limitations arise on the one hand from constraints on the physically possible control effort, and on the other hand from the right-half-plane zeros corresponding to the approximation of the time delay θ in the nominal model. It can be shown that for systems with time delays the closed-loop bandwidth is limited to be less than $1/\theta$ (Ref. 12). Due to these limitations, a bandwidth of about $\omega_B \approx 2.7$ rad/s or 0.43 Hz is achieved when just considering the feedback part of the controller, as can be seen from Figure 9. Here, the bandwidth ω_B is defined as the frequency where the Sensitivity S crosses the -3dB line for the first time from below. Note that the feedback controller shows a worse performance than the uncontrolled case in a frequency band above approximately 0.7 Hz. This can be explained by the so called second waterbed formula, which is based on a weighted sensitivity integral[12]. It states that reducing the sensitivity of a plant with right half-plane (RHP) zeros at low frequencies will cause a large peak in the sensitivity over a limited frequency range.

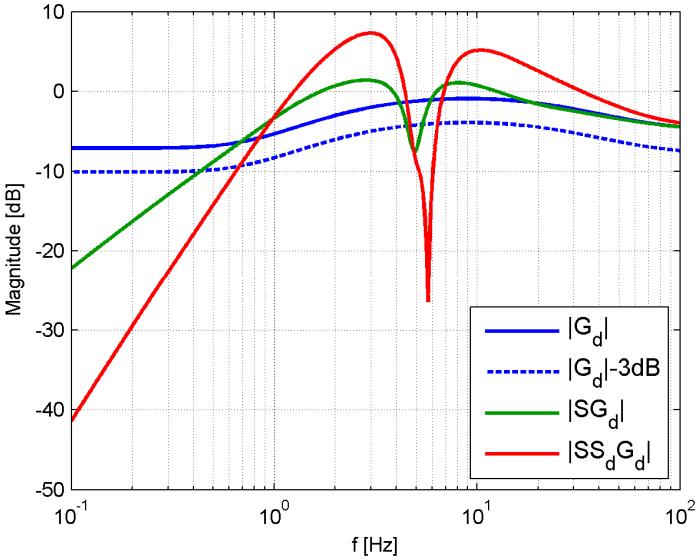

Figure 9. Frequency response of the plant output to sinusoidal disturbances in the flow speed for the uncontrolled plant (blue line), the feedback controlled plant (green line) and the feedback controlled plant augmented by a feedforward disturbance compensation (red line).

Since the input d to the disturbance model G_d can be measured online, the bandwidth can be improved by using a feedforward controller K_d, which is calculated by

$$K_d = G_F \tilde{G}_n^{-1} G_d . \qquad (7)$$

Herein $\tilde{G}_n$ denotes the allpass-free part of the nominal plant model to yield a stable inverse, and G_F represents a fast first order filter to render the transfer function K_d causal. Figure 9 shows that the feedforward controller increases the bandwidth of the controlled plant with respect to the measured disturbances to about 0.7 Hz. However, this comes at the price of increasing the sensitivity even further at a frequency band above approximately 0.8 Hz.

E. Closed Loop Control Results

The performance of the controller is evaluated by subjecting it to a pseudo-random velocity signal (PRS). The voltage signal to the shutters is constructed of pseudo-random amplitude steps summed with pseudo-random amplitude sinusoidal signals of frequencies less than 1Hz. The velocity input has a bandwidth of approximately 1Hz. Figure 10 a) shows the magnitude of the velocity plotted against time, and b) shows the power spectrum magnitude of the velocity plotted against frequency. The velocity ranges from a minimum of 6.25m/s to a maximum of 7.25m/s with the mean flow speed of 6.9m/s. The same signal is repeated 15 times to reduce the uncertainty in the amplitude

of the power spectrum to below 26% and the resulting time series measurements are averaged to reduce uncorrelated measurement noise.

The controller is commanded to maintain a constant reference lift of 1.8N during the PRS experiments. The reference lift is above the maximum value of the uncontrolled lift, this was done to reduce the effect of measurement noise. Figure 11 shows the averaged experimental controlled and uncontrolled lift force time series along with

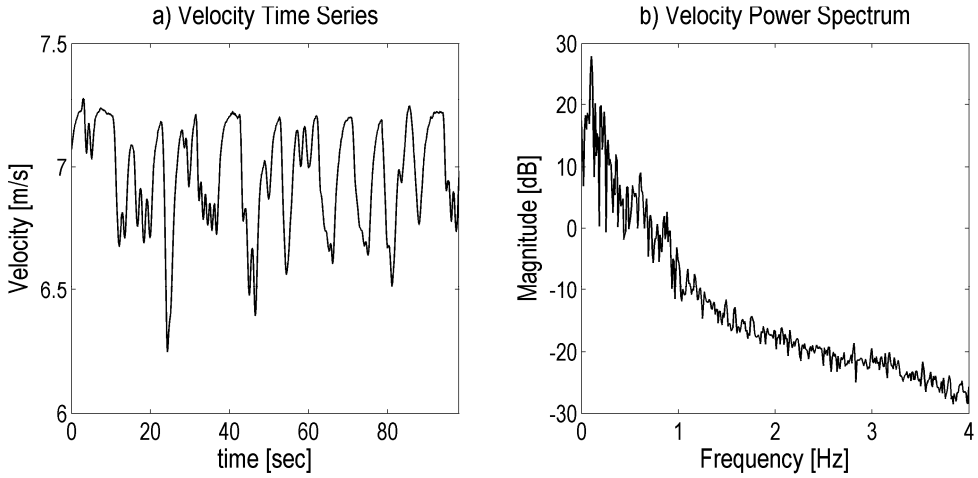

Figure 10. a) Measured pseudo random velocity time series and b) power spectrum used to test controller

simulation results and the desired lift force. The simulation results are obtained using the averaged, experimentally measured velocity profile as an input to the disturbance model and the same reference lift from experiment. The resulting signals are passed through the closed loop and feed forward disturbance controllers and the plant model response to actuation. Without control the lift reaches a minimum of 1.1N and a maximum of 1.5N. With control the lift ranges from 1.7N to 1.88N, where the minimum is from a point where the actuator input is saturated and the required change in lift exceeds the maximum possible value.

Figure 12 shows the power spectrum magnitude of the controlled and uncontrolled lift fluctuations plotted against frequency. Fifteen records of the length of an entire period of the pseudo-random velocity signal are used in calculating the power spectrum giving an uncertainty in the peaks in the spectrum of less than 26% and a frequency resolution of approximately 0.01Hz.

IV. Discussion of Results

The simulation results, shown in figure 11, agree well with the experimental results suggesting that the unsteady aerodynamics and dynamics of the response to pressure actuation are captured well by the linear, black-box, models even though the underlying process is highly complex and nonlinear. The black-box models reduce the infinite dimensional system from the solution of the Navier-Stokes equations to a single input-single output system (SISO). This also suggests that the linear superposition of the response to actuation and the response to the time varying velocity has validity for practical controller synthesis. The use of linear models enables the use of a

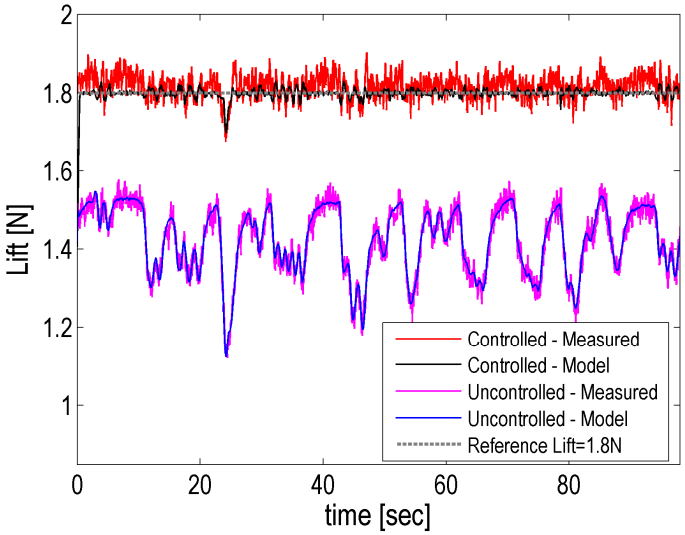

Figure 11. Phase averaged controlled and uncontrolled lift time series and comparison with model(s) (disturbance model in uncontrolled case and plant model, disturbance model and controllers in controlled case).

wide range of relatively simple controller synthesis techniques and analysis tools.

The controller is effective at reducing lift fluctuations at low frequencies, less than ~0.8 Hz (k=0.08), but begins to amplify disturbances above this frequency. The Bode integral formula shows that noise attenuation over some frequency band is accompanied by noise amplification over some other frequency band for systems with a pole excess of at least two[12]. Ideally this range of frequency amplification would occur at frequencies too fast for the plant to respond at, but for systems with RHP zeros more severe limitations apply. A weighted sensitivity integral shows that the amplification of disturbances must occur over a limited frequency range. Because of the time delay present in the plant modeling which can be approximated by an all-pass transfer function containing RHP zeros and the disturbance model this amplification occurs from ~1Hz (k=0.09) to ~5.5Hz (k=0.5). The sensitivity of the two-degree of freedom controller used in experiment is given by SS_D (Ref. 12). The controller is capable of suppressing disturbances while the overall sensitivity is below 1 (0dB) and disturbances are amplified when the overall sensitivity is greater than 1. Figure 9 shows the overall sensitivity of the modeled plant and disturbance and the point where the overall sensitivity crosses 1 from below is near 1Hz and crosses 1 from above at 5.5Hz. This agrees with the experimentally obtained power spectrum of lift fluctuations where the controlled disturbances are amplified over the uncontrolled fluctuations, again suggesting that the linear models capture the dynamics well.

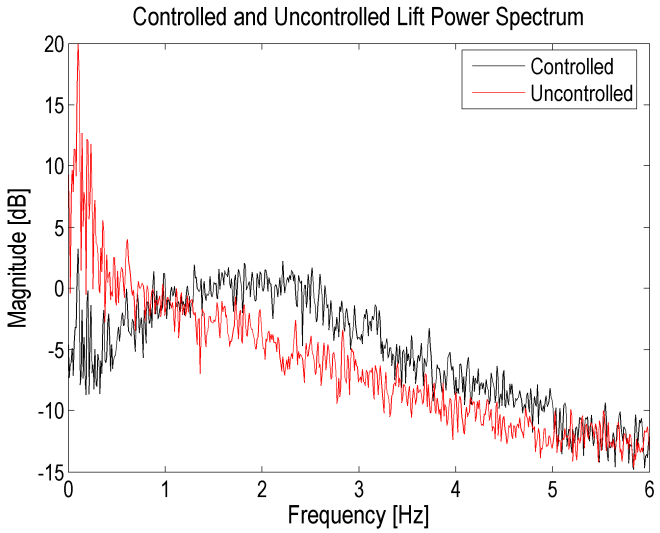

Figure 12. Power spectrum comparison of fluctuating lift force during controlled and uncontrolled pseudo random velocity input at design conditions.

The nominal time delay from desired pressure input to jet velocity is 0.023 seconds (t^+≈0.8) while the nominal time delay from desired pressure to lift increase is 0.157 seconds (t^+≈5), suggesting a time delay from jet velocity to the initiation of lift increase of t^+≈4. This is believed to be due to the time for a disturbance issued from the actuators to roll up and convect over the wing. This method of actuation does not show the initial decrease in normal force, circulation or lift as seen in Ref. 1-3. This is believed to be due to the first order model behavior of the jet velocity obtained by a desired step increase in pressure as opposed to the step increase in jet velocity observed while maintaining a constant pressure within the wing's plenum, which does show an initial decrease in lift[3]. This fluid dynamic time delay limits the bandwidth of possible control, as discussed above.

The relatively low bandwidth of the pressure regulator and the time delay between step inputs of desired pressure to jet velocity raises the question, if a faster actuator is used would the bandwidth of control be increased? Comparisons with a zero-net-mass-flux (ZNMF) wing with piezoelectric actuators shows negligible time delay between a desired input signal and measured output of jet velocity. Consequently, the jet velocity bandwidth of the piezoelectric actuators is an order of magnitude larger than the pulsed-blowing wing's jet velocity. The ZNMF wing does show the initial decrease in lift (non-minimum phase behavior) as observed by Ref. 1-3. The non-minimum phase behavior implies a right half plane (RHP) zero in the transfer function. A RHP-zero imposes control limitations at *either* low *or* high frequencies[12]. One can achieve tight control at frequencies below approximately $z/2$, where z is the magnitude of the RHP-zero or at frequencies above $2z$ by reversing the sign of the controller gain. Black-box models of PRBS voltage inputs to the piezoelectric actuators, which agree well with measured data, show a peak undershoot at t^+≈1.2 and have a RHP-zero located at 16.5 (Ref. 15). This zero implies the ability to achieve control below f≈1.3Hz (k=0.12) or control above f≈5.3Hz (k=0.48), which is comparable to the region where disturbances are amplified with the pulsed-blowing wing modeled with a pure time delay. As a result, even with faster actuators, *the range of frequencies of possible control is limited by the fluid dynamic response to actuation, not the bandwidth of the actuators.*.

The first order models with a time delay fit the measured data much better than the previous modeling with first order models[9]. The improved modeling leads to a better agreement between experiment and theory. The range of frequencies of the current controller is increased over the range in Ref. 9. This is on the one hand due to the

incorporation of an unsteady aerodynamic model and the feedforward disturbance compensation. On the other hand the better modeling also improves the performance.

V. Conclusions

The current effort to suppress lift oscillations in an unsteady freestream was successful. The controller shows reductions in the fluctuating lift at frequencies $k<0.09$.

The linear models are capable of predicting the lift response to pressure actuation and unsteady aerodynamics, which can be seen by the comparison between the experimental and simulation results. Additionally, the assumption of linear superposition of the response to pressure actuation and the "gusting" velocity is valid within practical, control design limitations.

The understanding and modeling of the unsteady aerodynamics associated with "gusting" conditions is necessary for control of a flight vehicle. Linear, black-box models provide a practical means for modeling the response to "gusting" in absence of a suitable theoretical model for low aspect ratio, low Reynolds number separated flow conditions.

The bandwidth of control is shown to be limited by the separated flow's response to actuation, not the bandwidth of the actuator. The time delay present in the system is responsible for limiting the bandwidth. This time delay is related to the time for the disturbance created by the actuators to convect over the wing and establish the new flow field that leads to an increase in lift. Even with faster actuators, the RHP-zero limits the control over a similar range of frequencies to the pulsed-blowing wing. These results suggest an upper limit on the frequency response that can be achieved on a wing using AFC.

Acknowledgments

The support for this work by the U.S. Air Force Office of Scientific Research MURI (FA9550-05-0369) with program manager Dr. Fariba Fahroo and AFOSR Grant (FA9550-09-1-0189) monitored by Dr. Doug Smith is gratefully appreciated. David Williams gratefully acknowledges partial support from the Alexander von Humboldt foundation. We also acknowledge the partial support from the Illinois NASA Space Grant Consortium for Wesley Kerstens.

References

[1]Darabi, A., and Wygnanski, I., "Active management of naturally separated flow over a solid surface. Part 1. The forced reattachment process," *J. Fluid Mech*. 510, 2004, pp.105-129.

[2]Brzozowski, D. and Glezer, A., "Transient Separation Control using Pulse Combustion Actuation," AIAA paper 2006-3024, 3rd Flow Control Conf., 5-8 June 2006, San Francisco, California.

[3]Williams, D.R., Tadmor, G., Colonius, T., Kerstens, W., Quach, V., and Buntain, S. The lift response of a stalled wing to pulsatile disturbances. *AIAA J.* Vol. 47, 2009.

[4]Greenberg, J., "Airfoil in Sinusoidal Motion in a Pulsating Stream," NACA-TN-1326, 1947

[5]Theodorsen, T., "General Theory of Aerodynamic Instability and the Mechanism of Flutter," NACA-TR-496, 1949

[6]Williams, D.R., Quach, V., Kerstens, W., Buntain, S., Tadmor, G., Rowley, C., Colonius, T., "Low-Reynolds Number Wing Response to an Oscillating Freestream with and without Feed Forward Control," AIAA Paper 2009-143, 2009.

[7]Leishman, J., *Principles of Helicopter Aerodynamics*, 1st ed., Cambridge Aerospace Series, Cambridge, England, UK, 2000

[8]van der Wall, B., "The Influence of Variable Flow Velocity on Unsteady Airfoil Behavior," DLR-FB 92-22, 1992

[9]Williams, D.R., Kerstens, W., Pfeiffer, J., King, R., Colonius, T., "Unsteady Lift Suppression with a Robust Closed Loop Controller". In R. King(Ed), *Active Flow Control II*, NNFM 108, Springer, 2010, pp.19-30

[10]Frank, "Optimale Allpassapproximation von Totzeitgliedern im Zeitbereich", at – automatisierungstechnik 44, 1996, pp.42-43

[11]Park, J.-K. & Choi, C.-H., "Dynamic compensation method for multivariable control systems with saturating actuators," *IEEE Transactions on Automatic* Control 40, 1995, pp.1635-1640

[12]Skogestad, S., Postlethwaite, I., *Multivariable feedback control – Analysis and design*, John Wiley & Sons, Chichester, England, 1996.

[13]Henning, L., Pastoor, M., King, R., Noack, B., Tadmor, G., "Feedback Control Applied to the Bluff Body Wake," R. King (Ed.), *Active Flow Control*, NNFM 95, Springer, 2007, pp.369-390.

[14]Heinz, N., King, R., Gölling, B., "Robust Closed-Loop Lift Control on an Industry-Relevant Civil Aircraft Half Model," R. King (Ed.), *Active Flow Control II*, NNFM 108, Springer, 2010, pp.125-139

[15]Quach, V., Kerstens, W., Williams, D., Tadmor, G. and Colonius, T., "Transient Response of a Wing to Arbitrary Actuator Input," ICJWSF Sep. 2010 [Unpublished].